Effect of Chain Conformational Change on Micelle Structures: Experimental Studies and Molecular Dynamics Simulations

Weiwei Ding, Shaoliang Lin, Jiaping Lin,* and Liangshun Zhang

Key Laboratory for Ultrafine Materials of Ministry of Education, School of Materials Science and Engineering, East China University of Science and Technology, Shanghai 200237,China

Received: August 29, 2007; In Final Form: October 30, 2007

The effect of chain conformation change on the self-assembly behavior of poly(γ-benzyl- L-glutamate)-*block*-poly(ethylene glycol) (PBLG-*b*-PEG) was studied both experimentally by transmission electron microscopy, laser light scattering, and circular dichroism and computationally using molecular dynamics (MD) simulation. It was found that, by introducing trifluoroacetic acid to the PBLG-*b*-PEG solution, the conformation of the PBLG chain transforms from α-helix to random coil, which results in a change of the micelle structures formed by PBLG-*b*-PEG from rod to sphere. Meanwhile, the MD simulations were performed by using Brownian dynamics on the self-assembly behavior of model AB-type diblock copolymers with various chain rigidities of the A-block. The results show that, by decreasing the fraction of rigid chain conformation of the A-block, which corresponds to the helix−coil transition in the PBLG-*b*-PEG sample, the aggregate structure transforms from rod to sphere. The MD simulations also provide chain packing information in the micelles. On the basis of both experimental and MD simulation results, the mechanism regarding the effect of the conformation change of the polypeptide block copolymer on its self-association behavior is suggested.

Introduction

Amphiphilic copolymers are a family of materials suitable for use as building materials for the formation of supramolecular structures.[1−7] Recently, various micelle morphologies such as spheres, rods, vesicles, tubules, and cylinders have been observed for block copolymers.[8−12] To make these self-assembled systems useful for specific applications such as sensors, nanoreactors, drug delivery, and so forth, great efforts have been made to find out the factors that affect the formation of these nanostructures and the transitions among them. Investigations of the mechanism toward the self-association behavior of the amphiphilic block copolymers are also very desirable.[13−17]

The conformation of the polymer chains is an important parameter in determining the nanostructures of block copolymers. Polypeptide is a good model system because of its well-defined chain conformations of high order, such as α-helix, which imparts rod-like character and can be converted into a random coil conformation under certain conditions.[18] Such structural features make the polypeptide-based copolymer an informative sample for studies of self-assemblies.[19−22] For example, Lecommandoux et al. reported the formation of schizophrenic vesicles based on a zwitterionic diblock copolymer poly(L-glutamic acid)-*block*-poly(L-lysine).[20] The hydrophobicities of the two polypeptide blocks vary with changes of pH value in aqueous medium, leading to the formation of vesicles with different supramolecular structures. Schlaad et al. investigated the aggregation behavior of polybutadiene-*block*-poly(L-glutamate)s in dilute aqueous solutions.[21] It was found that the block copolymers can form either spherical micelles or large vesicular aggregates. The size and structure of the aggregates depend on the chemical composition of the block copolymers. Thünemann et al. studied the self-assembly behavior of symmetric linear ABCBA pentablock copolymers consisting of poly(ethylene oxide), poly(γ-benzyl-L-glutamate) (PBLG), and poly(perfluoro ether).[22] It was found that they can form two-compartment micelles of mainly cylindrical shape in aqueous solution. The poly(perfluoro ether) (C blocks) forms the liquid-like center of the micelles, and it is surrounded by a first shell consisting of PBLG (B blocks) and a second shell of poly(ethylene oxide) (A blocks). By combining the experimental measurement with the conformation analysis of PBLG blocks, a reasonable precise nanostructure with the thickness of each micelle shell was proposed.

However, so far, limited work has been concerned with the effect of chain conformation change on the self-assembly behaviors of polypeptide copolymers, especially in organic solvent. Babin et al. recently reported the formation of stimuli-responsive micelles from polyisoprene-*b*-poly(L-lysine) copolymers in water.[23] The micelle structures vary with pH value and ionic strength. This has been explained by the conformational transition in the polypeptide chains. In acidic conditions, the corona-forming poly(L-lysine) block is charged and therefore in its coil conformation, leading to large micellar size. On the contrary, when pH increases, the polypeptide undergoes transition to an α-helical conformation, and the aggregate size decreases.

PBLG-based copolymers are one of the most important branches of polypeptides. It is well-known that PBLG takes an α-helix conformation and behaves as a rod-like segment in neutral organic solvent. This secondary structure can be combined with the coiled conformation of synthetic segments, such as poly(ethylene glycol) (PEG), to form rod−coil block copolymers.[24] When a denaturant organic acid such as trifluoroacetic acid (TFA) is introduced, the conformation of PBLG transforms from helix to random coil.[18,25−27] The block copolymer with coil−coil structure can be achieved. The unique

* Corresponding author. Tel: +86-21-64253370. Fax: +86-21-64253539. E-mail address: jplinlab@online.sh.cn.

10.1021/jp076939p CCC: $40.75
Published on Web 12/23/2007

properties of being biocompatible and biodegradable and the ability to self-assemble and undergo conformation transition under certain conditions make them potential candidates for applications in nanotechnology and medicine and good models for fundamental research.

Recently, computer simulation has emerged as a powerful tool to investigate the self-assembly behavior of amphiphilic copolymers.[28−39] Molecular dynamics (MD) simulation has widely been utilized to characterize the aggregation behavior of the amphiphilic copolymers because the obtained computational results are straightforward compared with the experimental findings.[30−32] Many simulation studies based on MD simulations have been performed on the self-assembly behavior of block copolymers consisting of flexible coil chains.[33−35] For the rod−coil block copolymers, so far, most studies are focused on the liquid−crystalline behavior in bulk.[36−38] Recently, our group studied the self-assembly behavior of amphiphilic rod−coil diblock copolymers and investigated the micelle structure and molecular packing by performing MD simulations using Brownian dynamics.[39] The results show that micelles with various structures such as disk and string can be formed by the rod−coil diblock copolymers. Influences of rod pair interaction and chain length on the self-assembly behavior have been studied. The aggregate structure can transform from disk to string and further to some small broken aggregates with increasing segregation strength of the rod pairs. It is also interesting to further investigate the effect of chain rigidity change, which is manifested by the helix−coil transition in the present work, on the aggregate structures.

In this work, we studied the effect of chain conformation change on the self-assembly behavior of PBLG-*b*-PEG by transmission electron microscopy (TEM), laser light scattering (LLS), circular dichroism (CD), as well as simulation. It was found that the conformational change from α-helix to random coil of PBLG chains leads to a rod-to-sphere structure transition of micelles formed by PBLG-*b*-PEG. Simulations on the self-assembly behavior of model AB-type diblock copolymers also indicated that, by decreasing the fraction of rigid chain conformation of the A-block, which corresponds to the helix−coil transition in the PBLG-*b*-PEG sample, the aggregate structure transforms from rod to sphere. By combining both experimental and MD simulation results, the mechanism regarding the effect of the conformation change of the polypeptide block copolymer on its self-association is proposed.

Experimental Section

Materials. Methoxypolyethylene glycol amine (M_w = 20 000) was purchased from Sigma, Inc., and dissolved in toluene in a flame-dried reaction bottle, followed by removal of the toluene in high vacuum to obtain the sample used for copolymer synthesis. Hexane, tetrahydrofuran, and 1,4-dioxane were of analytical grade and were refluxed with sodium and distilled immediately before use. The reagents used in the preparation of micelles such as chloroform, ethanol, and TFA were all spectroscopic grade. The other solvents were of analytical grade and used without further purification.

Synthesis of Polypeptide Block Copolymer. PBLG block copolymer was prepared by a standard *N*-carboxyanhydride (NCA) method.[18,25] *N*-carboxyl-γ-benzyl-L-glutamate anhydride was synthesized from triphosgene and γ-benzyl-L-glutamate. A well-purified NCA was polymerized in 3 wt % 1,4-dioxane solution by using methoxypolyethylene glycol amine (M_w = 20 000) as an initiator for 72 h at room temperature under a dry nitrogen atmosphere. The reaction mixture was poured into a large volume of anhydrous ethanol. The precipitated product was dried under vacuum and then purified twice by repeated precipitation from a chloroform solution into a large volume of anhydrous methanol. The block copolymer molecular weight was estimated by nuclear magnetic resonance (NMR) measurements (Avance 550). It was calculated by the peak intensities of the methylene proton signal (5.1 ppm) of polypeptide and the ethylene proton signal (3.6 ppm) of PEG in the ^{1}H NMR spectrum. According to the NMR analysis, the molecular weight of the block copolymer is 158 000.

Preparation of Micelles of Polypeptide Block Copolymer. To prepare the micelle solutions, the obtained PBLG-*b*-PEG sample was first dissolved in $CHCl_3$/TFA mixed solvents with various TFA contents. The polymer concentration of the initial solution was maintained at 0.083 g/L. Then ethanol, the selective solvent for PEG, was added at a rate of 1 drop every 3−4 s with vigorous stirring. In all the cases, the ethanol was added until the polymer concentration became 0.025 g/L. The obtained micelle solutions were stabilized at 25 °C for 48 h before the measurements. The samples for LLS measurements were kept in the optical light scattering cell and sealed before the stabilization.

Transmission Electron Microscopy. The morphologies of the micelles were examined by TEM (JEM-1200-EXII). Drops of micelle solution were placed on a carbon film-coated nickel grid, and were then dried at room temperature. Before the observations, the sample was stained by phosphotungstic acid ethanol solution (0.5 wt %). The TEM bright field imaging was performed with 120 kV accelerating voltage.

Light Scattering Measurements. The structure of the aggregates was characterized by combining dynamic light scattering (DLS) and static light scattering (SLS) measurements, which were performed on a commercial LLS spectrometer (ALV/CGS-5022) equipped with an ALV-High QE APD detector and an ALV-5000 digital correlator using a He−Ne laser (the wavelength λ = 633 nm) as the light source. All the measurements were carried out at 25 °C.

In DLS measurements, the Laplace inversion of a measured intensity−intensity time correlation function $G^{(2)}(t,q)$ in the self-beating mode can result in a line width distribution $G(\Gamma)$. For a pure diffusive relaxation, Γ is related to the translational diffusion coefficient D by $(\Gamma/q^2)_{C\to 0,q\to 0} \to D$ or a hydrodynamic radius distribution $f(R_h)$ via the Stokes−Einstein equation:

$$R_h = k_B T/(6\pi\eta D) \tag{1}$$

where k_B, T, and η are the Boltzmann constant, the absolute temperature, and the solvent viscosity, respectively. In this study, at a given concentration C, $(\Gamma/q^2)_{\varphi\to 0}$ or D of the micelles was calculated from the slope by extrapolating q^2 to 0, where q is the magnitude of the scattering wave vector [$q = (4\pi n/\lambda)\sin(\varphi/2)$] as a function of the scattering angle φ, the solvent refractive index n of the solution, and the wavelength λ of the incident beam. Then the hydrodynamic radius R_h of the micelles at a given polymer concentration can be further calculated from eq 1.

The radius of gyration R_g was calculated from SLS. On the basis of SLS theory, for a relatively highly dilute macromolecule solution at polymer concentration C (g/mL) and at scattering angle φ, the angular dependence of the excess absolute average scattered intensity, known as the excess Rayleigh ratio $R_{VV}(q)$, can be approximated as

$$KC/R_{VV}(q) = 1/M_w[1 + (R_g^2 q^2)/3] + 2A_2C \tag{2}$$

TABLE 1: Conversion of the Reduced Unit System[a]

reduced unit	value
reduced length	$1\sigma = 0.4$ nm
reduced energy	$1\epsilon = 0.5$ kJ/mol
reduced mass	$1m = 23.3 \times 10^{-27}$ kg
reduced temperature	$1T_0 = \epsilon/R = 60.1$ K
reduced time	$1t = \sqrt{A_v m\sigma^2/\epsilon} = 2.12$ ps
reduced density	$1\rho = m/\sigma^3 = 0.363$ g/cm^3
reduced pressure	$1P = \epsilon/(A_v\sigma^3) = 13.0$ MPa

[a] R is the gas constant, and A_v is Avogadro's number.

where A_2 is the second virial coefficient, M_w is the weight-average molecular weight, and K is the optical constant and is equal to $4\pi^2n^2(dn/dC)^2/(N_A\lambda^4)$, with N_A being Avogadro's number and dn/dC being the specific refractive index increment. For a dilute polymer solution, eq 2 can be simplified to

$$KC/R_{VV}(q) \approx 1/M_w[1 + (R_g^2q^2)/3] \quad (3)$$

From eq 3, the apparent radius of gyration R_g was calculated from the plot after $R_{VV}(q)$ was measured at a series of φ values from 30° to 120°. The details of LLS instrumentation and theory can be found elsewhere.[40−42]

Circular Dichroism. CD analysis of the conformation of polypeptide blocks was performed with a JASCO J-810 spectrometer. The micelle solutions were introduced in quartz cells with 1 cm optical path length and measured at room temperature.

Method of MD Simulation

The simulations were carried out by using the simulator, coarse-grained MD program COGNAC of OCTA. The simulator was developed by Doi's group, and is available to the public on the OCTA website.[43] COGNAC uses the reduced unit system for setting data. To convert it to real units, a set of unit parameters, such as reduced length, reduced energy, and reduced mass, are given in Table 1. Other reduced quantities can thus be calculated from these unit parameters and are also presented in Table 1.

To construct an AB-type block copolymer capturing the essential features of the polypeptide-*b*-PEG rod−coil type diblock copolymer molecule, potentials that should be given are bonding potential, U_{mol}, and nonbonding potential, U_{ij}. That is, the potentials that act on the beads (atoms) are divided into two parts. The former can construct a desired molecule from atoms, while the latter describes intermolecular interactions.

The AB-type diblock copolymer molecule is represented by a linear chain consisting of several beads connected by bond stretching potential. In this work, an A-block with eight beads and a B-block with nine beads, coded as A_8B_9, is constructed. The illustration of this copolymer molecule model is shown in Figure 1. The beads colored blue and green are the hydrophobic A-block with variable chain conformation, i.e., rod or coil, and the hydrophilic B-block with flexible form, respectively. To realize the A-block with rigid form, angle bending potential is combined to keep the rigidity of the molecule. Without angle bending potential constraint, the B-block is represented by a flexible chain as shown in Figure 1. Therefore, U_{mol} is a combination of $U_{bond}(r)$ and $U_{angle}(\phi)$. $U_{bond}(r)$ is a function of the distance between the chemically bonded beads r. A harmonic type is applied and defined by

$$U_{bond}(r) = \frac{1}{2}k_b(r - r_0)^2 \quad (4)$$

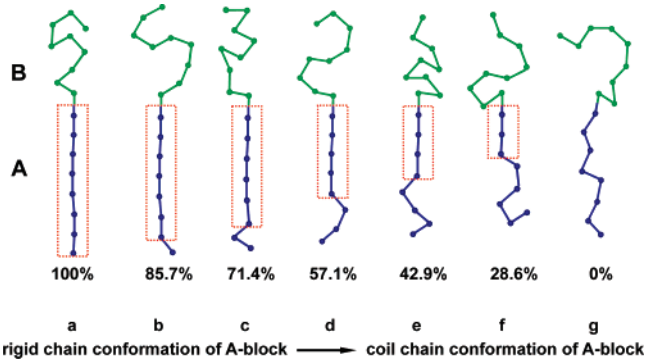

Figure 1. Layouts of an A_8B_9 diblock copolymer with the A_8 block transitioning from rigid to flexible chain form. The beads colored blue and green are the hydrophobic block and hydrophilic block, respectively. The percentages of the rigid conformation of A-block are presented below the copolymer schemes.

where k_b is the bond spring constant, and r_0 is the equilibrium bond length. The value of k_b is set to be 10 000, which is large enough to avoid the over-stretching of bonds, for both A- and B-blocks. $U_{bond}(r)$ consists of the potentials of the A-block, the B-block, and the junction bond of these two blocks. The set values of bond length r_0 are 0.75, 1.0, and 1.0 for them, respectively. Such a construction corresponds to the component of the PBLG-*b*-PEG sample studied in the present work. According to the NMR analysis, the length ratio of the PBLG block and the PEG block is about 0.57, which is close to the A-block-to-B-block length ratio of 0.66 for the A_8B_9 copolymer.

For the A-block, the angle bending potential, $U_{angle}(\phi)$, is a cosine harmonic function of the angle ϕ defined by the three chemically connected beads:

$$U_{angle}(\phi) = \frac{1}{2}k_a(\cos\phi - \cos\phi_0)^2 \quad (5)$$

where k_a is the angle spring constant, and ϕ_0 is the equilibrium angle. The larger the k_a value, the more rigid the molecule chain. To realize an A-block with rigid form, the equilibrium angle ϕ_0 is set to a value of 0.1° (substantially zero). The constant k_a is set to be 10 000. Without angle bending potential constraint, the A-block becomes a coil.

The interaction energy U_{ij} is given by the standard Lennard-Jones (LJ) 12:6 potential U_{ij} acting between any pair of beads i and j:

$$U_{ij} = \begin{cases} 4\epsilon_{ij}\left[\left(\frac{\sigma_{ij}}{r_{ij}}\right)^{12} - \left(\frac{\sigma_{ij}}{r_{ij}}\right)^{6} - \left(\frac{\sigma_{ij}}{r_{ij}^c}\right)^{12} + \left(\frac{\sigma_{ij}}{r_{ij}^c}\right)^{6}\right], & r \le r_{ij}^c \\ 0, & r > r_{ij}^c \end{cases} \quad (6)$$

where r_{ij}^c is the cutoff distance, and $r_{ij} = |\bar{r}_i - \bar{r}_j|$, with $\bar{r}_i$ and $\bar{r}_j$ being the locations of the ith and jth beads, respectively. The amphiphilicity in this model is realized using a method mentioned by Bhattacharya et al.[44,45] It is introduced by a repulsive cutoff distance for the A−B and B−B interactions ($r_{AB}^c = 2^{1/6}$, $r_{BB}^c = 2^{1/6}$), and an attractive cutoff for the A−A interaction ($r_{AA}^c = 2.5$). Such selections of r_{ij}^c make the A-block form the core of micelles. The diameter σ of LJ bead is kept at unity for any pair of species. The pairwise interaction ϵ_{AA} between A-beads is chosen to be 2.0, while the other interactions are all set to be unity, i.e., $\epsilon_{AB} = \epsilon_{BB} = 1.0$.

In this work, we focus on the influence of the chain conformation of a polypeptide block (i.e., the A-block in the simulations) on its self-assembly behavior. The AB copolymers

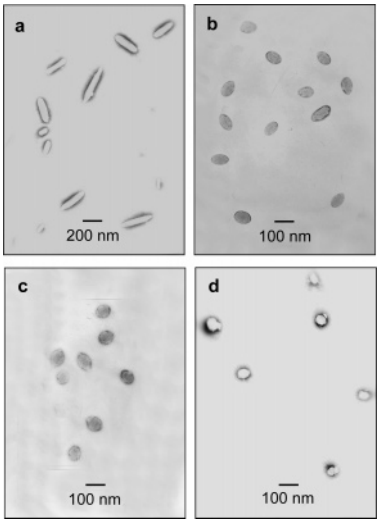

Figure 2. TEM photographs of the PBLG-*b*-PEG micelles formed in ethanol solutions with various TFA mole fractions: (a) 0; (b) 0.017; (c) 0.033; (d) 0.066.

with various chain conformations of the A-block, changing from rigid to flexible chain, are illustrated in Figure 1. The percentages (f_R) of the rigid conformation of A-blocks are also presented. Here, f_R is given by $(n-1)/(m-1)$, where n is the number of beads in rigid form within the A-block (shown in red rectangles in Figure 1) and m is the total number of the beads of the A-block.

All the simulations are carried out on a cubic cell ($60 \times 60 \times 60$) using a dynamic algorithm with temperature controlling method (NVT ensemble). Brownian dynamics is applied in this work, which was developed by Grest and Kremer.[46] To simulate a constant temperature ensemble, the beads are coupled to a heat bath, and the equations of motion are written by

$$m_i \frac{d^2\bar{r}_i}{dt^2} = \bar{F}_i - \Gamma_0 \frac{d\bar{r}_i}{dt} + \bar{W}_i(t) \quad (7)$$

where m_i is the mass of the ith bead. $\bar{F}_i$ is the force acting on ith bead, which is calculated by the potential energies consisting of U_{mol} and U_{ij} related to the location of the ith bead. Γ_0 is the friction constant. In the Langevin dynamics, the effect of solvent molecules is implicitly treated by the noise term $\bar{W}_i(t)$, which can be calculated using the fluctuation−dissipation relation:[44,47]

$$\langle \bar{W}_i(t) \cdot \bar{W}_j(t') \rangle = 6k_B T_0 \Gamma_0 \delta_{ij} \delta(t - t') \quad (8)$$

In order to minimize the effect of finite system size, periodic boundary conditions were imposed. A regular body-centered cubic (bcc) packing lamellar mode for 100 A_8B_9 copolymers is applied to generate the initial structures of molecules, and the structure relaxation is done by stochastic dynamic simulation. The different initial states of the simulation system have been examined to have no influence on the calculation results under the present conditions employed. In the calculation, the integration time step $\Delta t = 0.004$ was selected. The length of the simulation runs was 3×10^6 time steps, i.e., 12 000 time units, which insured that the simulated system reached equilibrium. All calculations were performed at a temperature of $T_0 = 3.0$.

Results and Discussion

Morphological Changes Observed by TEM. Figure 2 shows TEM photographs of aggregate morphologies formed by PBLG-*b*-PEG copolymers in solutions with various amounts of TFA.

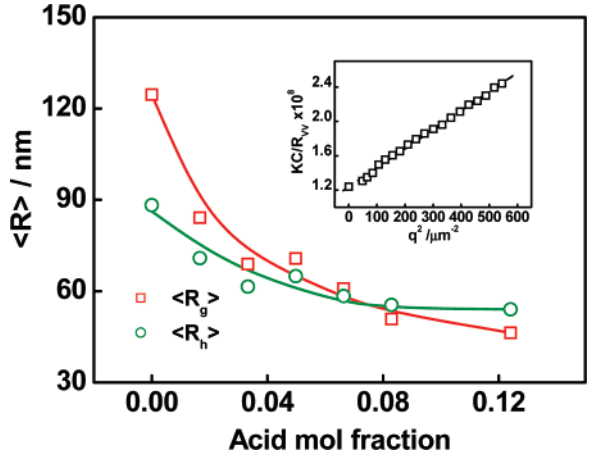

Figure 3. Plots of $\langle R_g \rangle$ and $\langle R_h \rangle$ versus the denaturant acid mole fraction of the PBLG-*b*-PEG micelle solutions. Shown in the inset is a typical plot for the angular dependence of the excess Rayleigh ratio $R_{VV}(q)$ for PBLG-*b*-PEG micelle solutions.

Micelles are formed when ethanol is added to desolvate the insoluble polypeptide blocks from solution. As shown in Figure 2a, without the acid, rod-like micelles appear. The length of the rods is in the range of 200−240 nm. The diameter is about 100 nm. When the denaturant organic acid TFA is introduced, the rods become shorter, as shown in Figure 2b. As the acid concentration further increases, the length of the rod decreases, and the micelles become spherical (Figure 2c). When the TFA mole fraction increases to 0.066, regular spheres are found in the TEM observations (Figure 2d). Further increasing the acid concentration has no effect on the aggregate morphologies. It is also noted from TEM observations that, concomitantly with the changes in the morphologies, the micelle size tends to be smaller.

Micelle Size and Structure Studied by LLS. The effect of acid on the morphology change of PBLG-*b*-PEG micelles was further studied by LLS. Figure 3 shows that both the average hydrodynamic radius ($\langle R_h \rangle$) and the average radius of gyration ($\langle R_g \rangle$) decrease markedly with increasing acid mole fraction in the range between 0 and 0.083. Shown in the inset is a typical plot for the angular dependence of the excess Rayleigh ratio $R_{VV}(q)$ for the PBLG-*b*-PEG micelle solution. The slope of $KC/R_{VV}(q)$ versus q^2 can lead to $\langle R_g \rangle$. As can be seen in Figure 3, the $\langle R_g \rangle$ decreases more sharply than $\langle R_h \rangle$ does. This is because that they are defined in different ways, namely, $\langle R_h \rangle$ is the radius of a hard sphere with the same translational diffusion coefficient and the same condition, while $\langle R_g \rangle$ reflects the density distribution of the chain in real physical space.[48] The sharp decrease of $\langle R_g \rangle$ can be attributed to the morphology change from long rod to sphere, which has also been observed by TEM. As the acid content further increases, both $\langle R_g \rangle$ and $\langle R_h \rangle$ level off, indicating that the effect of acid becomes less pronounced.

The micelle structure change can be also viewed in terms of the ratio of $\langle R_g \rangle$ to $\langle R_h \rangle$, which is sensitive to the particle shape.[49−51] It is well-known that $\langle R_g \rangle / \langle R_h \rangle$ decreases as the structure changes from an extended manner to a sphere, and, for a uniform nondraining sphere, the ratio is 0.774. As shown in Figure 4, $\langle R_g \rangle / \langle R_h \rangle$ decreases from 1.41 to 0.86 with increasing TFA mole fraction in the range between 0 and 0.12, indicating that the supramolecular structure changes and becomes more spherical at higher TFA content. Such light scattering results are in reasonable agreement with TEM observations.

Conformation Changes of Polypeptide Blocks Characterized by CD. It is well-known that PBLG is a strong α-helix former but can transform to random coil conformation when

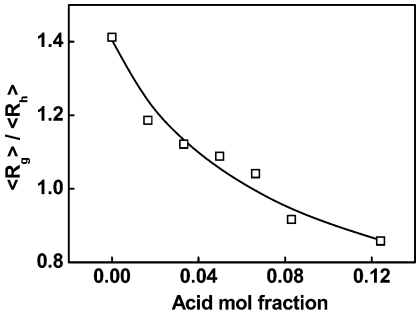

Figure 4. Plot of $\langle R_g \rangle / \langle R_h \rangle$ versus TFA mole fraction for the PBLG-*b*-PEG micelle solutions.

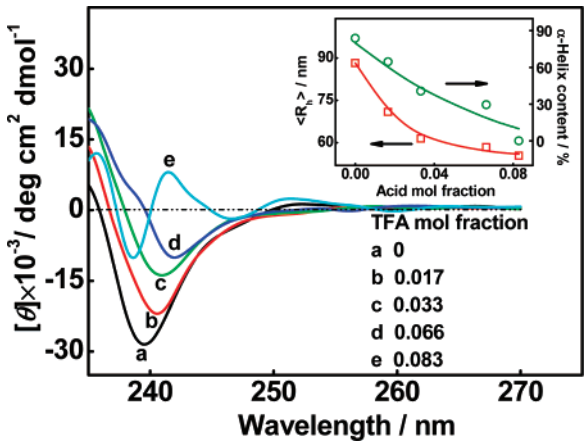

Figure 5. CD spectra for the PBLG-*b*-PEG micelle solutions with various TFA mole fractions. Shown in the inset are plots of the α-helix content and $\langle R_h \rangle$ versus the acid mole fraction.

TFA is introduced.[18,25−27] In this work, the PBLG secondary structure is characterized by CD, which is an effective way to determine the polypeptide conformation. The CD spectra recorded in micelle solutions with various TFA contents are shown in Figure 5.

The spectrum obtained from the micelle solution without TFA shows a negative minimum at 239 nm, indicating that the polypeptide adopts α-helix structure. It is noted that the wavelength of this peak is longer than the typical value of 222 nm reported for PBLG.[52] This band is widely reported to be assigned to the $n-\pi^*$ transition of peptide bonds, which can be influenced by many factors such as solvent, side chain, and intra- or intermolecular interactions.[53,54] In the present work, the red-shifted band in the CD spectra could be attributed to the aggregation of the PBLG blocks within the micelle core. Such an aggregation may change the environment that surrounds the PBLG chains, resulting in a peak position shift.[52] When the acid content is increased, the minimum peak shows a tendency of diminution, indicating that the amount of PBLG chains that take the α-helix conformation decreases. Upon further increasing TFA content, the typical spectrum of an α-helix secondary structure is substituted by a doubly inflected CD curve with a large minimum at 238 nm and a small positive maximum at 241 nm, which indicates that the polypeptide block adopts a random coil conformation.[21,55]

From the absolute value of molar ellipticity $[\theta]$ at the negative minimum, one can estimate the α-helix content according to the following equation:[56] helix content [%] $= ([\theta]_{obsd}/[\theta]_h) \times 100$, where $[\theta]_{obsd}$ is the measured molar ellipticity at peak wavelength λ_m, and $[\theta]_h$ is -34000 deg cm^2 dmol^{-1}. For comparison, plots of $\langle R_h \rangle$ and the α-helix content against the TFA mole fraction are shown in the inset of Figure 5. It is evident that, with increasing TFA mole fraction from 0 to 0.083,

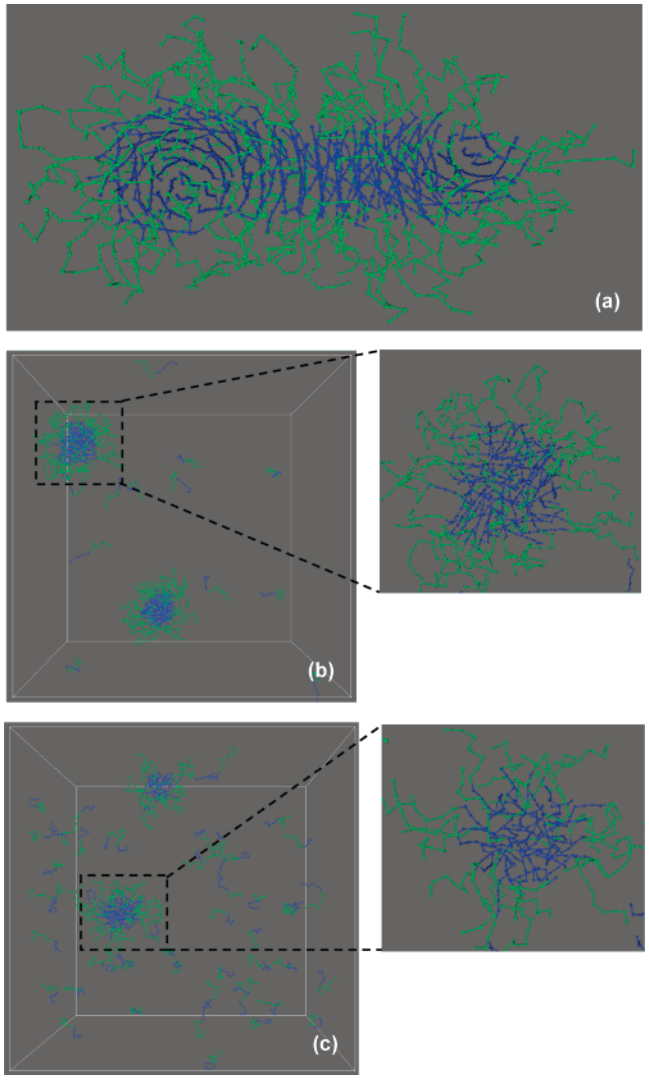

Figure 6. Typical snapshots of A_8B_9 copolymer systems with various percentages of the rigid conformation of the A-block: (a) $f_R = 100\%$; (b) $f_R = 71.4\%$; (c) $f_R = 42.9\%$.

the α-helix content of polymer chains decreases from 82% to 0, and the micelle size indicated by $\langle R_h \rangle$ decreases from 88 to 55 nm. The conformation and the morphological changes occur simultaneously. As the acid content is further increased, the conformation transition of the PBLG block no longer takes place; the micelle size also approaches a constant. The conformation transition is shown to be the key factor for the micelle structure change.

Computational Simulation. To visualize changes in micelle structure and molecular packing upon changing the chain conformation of A-blocks, typical snapshots of A_8B_9 copolymer aggregates are shown in Figure 6, where the A- and B-blocks are colored blue and green, respectively. The transition of polypeptide chain conformation from α-helix to random coil corresponds to the decrease of the rigid conformation fraction f_R in the A-block of the A_8B_9 copolymer. In the case of a full rigid conformation of the A-block, $f_R = 100\%$ (snapshot in Figure 6a), and a rod-like (cylinder-like) micelle is formed. Within the core, the rod blocks are interdigitated, and their long axes are aligned orientationally. The orientation vector is vertical to the micelle long axis and is gradually changed along the long-center-axis of the micelle to form a twisted structure. Such a rod-like aggregate structure was also observed for the block copolymer with different lengths in our previous work.[39] As

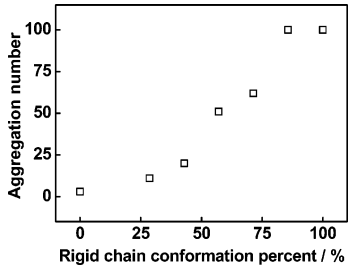

Figure 7. Plot of the largest aggregation number versus the percent of rigid chain conformation f_R of the A-block. The pairwise interaction ϵ_{AA} between rod beads is chosen to be 2.0.

the rigid chain conformation of the A-block, f_R, decreases, the rod-like micelle is broken into small aggregates coexisting with some single copolymers (unimers). Meanwhile, the chain packing within the core becomes less ordered. This can be seen from the snapshot at $f_R = 71.4\%$ in Figure 6b. With further decreasing f_R, more and more unimers come out of spherical aggregates, which results in a smaller size of spherical micelles. Meanwhile, a random packing of A-blocks can be observed at $f_R = 42.9\%$ in Figure 6c.

The findings from the snapshot pictures shown in Figure 6 indicate that the structure transforms from rod-like to spherical micelle upon decreasing the rigid chain conformation percentage of the A-block. Further more, the variation of the aggregation number concomitant with the shape change was also examined. Figure 7 shows the largest aggregation number as a function of percent of rigid chain conformation f_R of the A-blocks. As it is seen, when A-blocks take a highly rigid conformation ($f_R > 85.7\%$), the aggregation number is close to 100. Upon decreasing f_R, the aggregation number decreases dramatically. As the A-blocks take the coil conformation, the copolymers tend to assemble to form trimers or small aggregates. The decrease in the aggregation number shown in Figure 7 suggests that the micelle becomes smaller, since the smaller aggregation number leads to the smaller micelle size. This is in line with the TEM observations and DLS measurements.

Summarizing both the experimental findings and the simulation results, we propose the mechanism of micelle structure change induced by polypeptide conformation transition. Shown in Scheme 1 is a schematic illustration of PBLG-*b*-PEG micelles formed under different conditions. As evidenced by CD measurement, the polypeptide blocks within the micelle cores adopt a rigid α-helix conformation in the solution without TFA. The results obtained from MD simulation suggest that the full rigid rod blocks align in an orientation vector, and the vector is gradually changed along the long-center-axis of the micelle. This ordered twisted packing manner of rod blocks exhibits characteristics of the cholesteric liquid crystal structure, which is widely observed for α-helix PBLG in solution.[57] On the basis of both experimental and computational results, it is proposed that the polypeptide blocks within the cores are interdigitated and favor ordered parallel packing, with their long axis aligning in an orientation vector. The vector could gradually change along the long-center-axis of the micelle in a cholesteric liquid crystal manner, as shown in the partially expanded view of Scheme 1a. Such a packing of the PBLG blocks in the core satisfies the natural tendency toward twisted packing of helical rods and can also maximize the volume for the PEG blocks. The PEG segments relax, laterally forming the corona of the micelle to maximize their conformation entropy. In other words, the twisted structure is in favor of maximizing the entropy and minimizing the free energy. The helical structure of the PBLG rod packing was widely observed in the liquid crystal structure. When the

SCHEME 1: Schematic Representation of the Structure Change of a PBLG-*b*-PEG Micelle from (a) Rod to (b) Sphere Induced by the Helix-to-Coil Conformation Transition, and the Expanded View Schematically Depicting the Twisted Structure of PBLG Blocks with α-Helix Conformation in the Core of the Rod-like Micelle

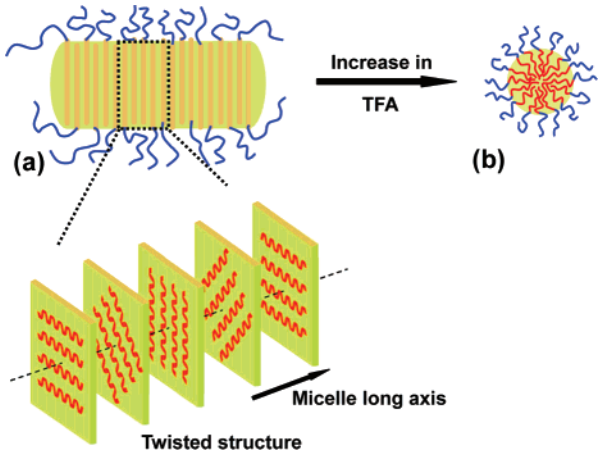

PBLG sample is dissolved in a solvent, cholesteric liquid crystal ordering forms above a critical polymer concentration. The polypeptide molecules align nearly parallel in a layer, and the layer stacks successively change the alignment direction by a constant angle around the normal of the layer. Like the helical supramolecular structure in the liquid crystal phase, the PBLG block packing in the rod-like micelle core can be described by the pitch of the twisted structure, which is equal to the distance of one rotating turn of orientation vector on the long axis.[39] The pitch of twisted packing is mainly determined by the balance between PEG repulsion and the order degree of PBLG blocks.

From another point of view, for PBLG in α-helix conformation, it is widely reported that every helix contains 3.6 amino acid units, and the screw-pitch is 0.54 nm. As for the sample studied in the present work, the molecular weight of the PBLG block is 138 000, and it should contain about 630 amino acid units, which corresponds to 175 helical turns. Therefore, the theoretical arithmetic result of the rod block length is about 94 nm for the block copolymer sample. Since the PEG coronas are collapsed during the preparation of the samples for the TEM observation, the thickness of the corona could be quite small with respect to the radius of the core. As a result, the observed micelle radius could be approximately equal to the radius of PBLG cores. It is about 100 nm from the TEM observations, close to the result we calculated for the length of the PBLG rod chain (94 nm). This phenomenon also supports the packing mode we proposed above, i.e., the PBLG rod blocks are arranged with their long axes parallel to each other within the micelle core.

Recently, Kim et al. observed a nanoribbon structure assembled by PBLG-*b*-PEG in toluene.[58] They proposed that the PBLG blocks are parallel to the plane of the ribbon, staking in a monolayer fashion. The PEG chains protrude outside and prevent the aggregation between the nanoribbons in the solution, while the length of the PBLG block used in our system is much longer than that of their sample. This expands the exposure of the hydrophobic rods at the edges of the micelles to ethanol, leading to a large energetic penalty associated with the assembly. This energetic cost of the edge exposure can be compensated by a twist of the PBLG blocks along the aggregate axis, which increases the available volume for the PEG blocks to maximize

the entropy of the PEG chains. As a result, a rod-like micelle with a twisted structure is formed. The twisted structure is an interesting finding of the present work. Further characterizations of the rod-like micelles, such as experimental characterization of the packing manner of the PBLG blocks in the core, would be helpful for more deep understanding of the self-assembly behavior of the polypeptide block copolymers.

When the denaturant acid TFA is added, the α-helix-to-coil conformation transition takes place, and the rigid chain conformation of the rod block decreases accordingly. As a result, the regular packing of PBLG blocks in the core is destroyed gradually, and the rod nanostructure can no longer be held up. To maintain a thermodynamic stable state, the spherical structure is preferred.[16] Such a transition mechanism is also revealed by the simulation. As rigid chain formation of the A-block decreases, the rod-like micelle is broken into small spherical micelles coexisting with some single polymers. Meanwhile, because of the extrication of some single copolymers, the aggregation number decreases markedly, and the size of the micelles decreases concomitantly.

When the acid content is increased to a certain value, the α-helix conformation transforms to random coil completely. Consequently, spherical micelles with coiled polypeptide blocks randomly packing inside the cores are formed as shown in Scheme 1b. Further increasing the TFA content has less marked effect on both morphology and size of the aggregates.

Conclusions

In summary, the effect of conformation transition on the self-assembly behavior of PBLG-*b*-PEG in ethanol medium was studied. Rod-like micelles with PBLG blocks, which adopt α-helix conformation, as the core and the PEG blocks as the corona are formed in ethanol solution without denaturant acid TFA. Such a rod-like morphology is also observed in MD simulation of model AB-type block copolymers with full rigid A-blocks. Because of the full rigid α-helix conformation, the rod blocks are expected to align in an orientation vector, which gradually changes along the long-center-axis of the rod. When TFA is added, a helix-to-coil conformation transition of the PBLG chain occurs, which results in the rod-to-spherical supramolecular structure change. Correspondingly, the aggregate morphology transition between the rod and sphere can be tailored by the rigidity of the A-block in the MD simulations. The accordance between the experiments and simulations supports the proposed mechanism that the helix−coil conformation transition of the polypeptide block copolymer exerts a marked effect on its self-assembly behavior. The helix−coil conformation transition of synthetic polypeptides, which is a simple model for proteins, is an interesting topic of studies. The further understanding of the influence of such intramolecular change on its supramolecular assembly could be helpful for knowing the behavior of more complex polypeptides and, by extension, protein systems.

Acknowledgment. This work was supported by the National Natural Science Foundation of China (50673026, 20574018). Support from the Doctoral Foundation of Education Ministry of China (Grant No. 20050251008), the Program for New Century Excellent Talents in University in China (NCET-04-0410), and the Project of Science and Technology Commission of Shanghai Municipality (05DJ14005, 06SU07002, and 0652nm021) is also appreciated.

References and Notes

(1) Harada, A.; Kataoka, K. *Science* **1999**, *283*, 65−67.
(2) Harada, A.; Kataoka, K. *Prog. Polym. Sci.* **2006**, *31*, 949−982.
(3) Won, Y.-Y.; Davis, H. T.; Bates, F. S. *Science* **1999**, *283*, 960−963.
(4) Jain, S.; Bates, F. S. *Science* **2003**, *300*, 460−464.
(5) Discher, B. M.; Won, Y.-Y.; Ege, D. S.; Lee, J. C.-M.; Bates, F. S.; Discher, D. E.; Hammer, D. A. *Science* **1999**, *284*, 1143−1146.
(6) Geng, Y.; Ahmed, F.; Bhasin, N.; Discher, D. E. *J. Phys. Chem. B* **2005**, *109*, 3772−3779.
(7) Tang, D.; Lin, J.; Lin, S.; Zhang, S.; Chen, T.; Tian, X. *Macromol. Rapid Commun.* **2004**, *25*, 1241−1246.
(8) Zhang, L.; Yu, K.; Eisenberg, A. *Science* **1996**, *272*, 1777−1779.
(9) Yu, Y.; Zhang, L.; Eisenberg, A. *Macromolecules* **1998**, *31*, 1144−1154.
(10) Zhang, L.; Eisenberg, A. *Macromolecules* **1996**, *29*, 8805−8815.
(11) Discher, D. E.; Eisenberg, A. *Science* **2002**, *297*, 967−973.
(12) Jenekhe, S. A.; Chen, X. L. *Science* **1998**, *279*, 1903−1907.
(13) Lokitz, B. S.; Convertine, A. J.; Ezell, R. G.; Heidenreich, A.; Li, Y.; McCormick, C. L. *Macromolecules* **2006**, *39*, 8594−8602.
(14) Li, Y.; Lokitz, B. S.; McCormick, C. L. *Angew. Chem., Int. Ed.* **2006**, *45*, 5792−5795.
(15) He, Y.; Lodge, T. P. *J. Am. Chem. Soc.* **2006**, *128*, 12666−12667.
(16) Bhargava, P.; Tu, Y.; Zheng, J. X.; Xiong, H.; Quirk, R. P.; Cheng, S. Z. D. *J. Am. Chem. Soc.* **2007**, *129*, 1113−1121.
(17) Wu, K.; Shi, L.; Zhang, W.; An, Y.; Zhang, X.; Li, Z.; Zhu, X. X. *Langmuir* **2006**, *22*, 1474−1477.
(18) Lin, J.; Liu, N.; Chen, J.; Zhou, D. *Polymer* **2000**, *41*, 6189−6194.
(19) Schlaad, H. *Adv. Polym. Sci.* **2006**, *202*, 53−73.
(20) Rodríguez-Hernández, J.; Lecommandoux, S. *J. Am. Chem. Soc.* **2005**, *127*, 2026−2027.
(21) Kukula, H.; Schlaad, H.; Antonietti, M.; Förster, S. *J. Am. Chem. Soc.* **2002**, *124*, 1658−1663.
(22) Thünemann, A. F.; Kubowicz, S.; von Berlepsch, H.; Möhwald, H. *Langmuir* **2006**, *22*, 2506−2510.
(23) Babin, J.; Rodriguez-Hernandez, J.; Lecommandoux, S.; Klok, H.-A.; Achard, M.-F. *Faraday Discuss.* **2005**, *128*, 179−192.
(24) Floudas, G.; Papadopoulos, P. *Macromolecules* **2003**, *36*, 3673−3683.
(25) Lin, J.; Abe, A.; Furuya, H.; Okamoto, S. *Macromolecules* **1996**, *29*, 2584−2589.
(26) Lin, J.; Lin, S.; Liu, P.; Hiejima, T.; Furuya, H.; Abe, A. *Macromolecules* **2003**, *36*, 6267−6272.
(27) Lin, J.; Lin, S.; Chen, T.; Tian, X. *Macromolecules* **2004**, *37*, 5461−5467.
(28) Zhang, L.; Lin, J.; Lin, S. *J. Phys. Chem. B* **2007**, *111*, 351−357.
(29) Zhang, L.; Lin, J.; Lin, S. *J. Phys. Chem. B* **2007**, *111*, 9209−9217.
(30) Schultz, A. J.; Hall, C. K.; Genzer, J. *J. Chem. Phys.* **2002**, *117*, 10329−10338.
(31) Schultz, A. J.; Hall, C. K.; Genzer, J. *Macromolecules* **2005**, *38*, 3007−3016.
(32) Alsunaidi, A.; Abu-Sharkh, B. F. A. *J. Chem. Phys.* **2003**, *119*, 9894−9902.
(33) Chushak, Y.; Travesset, A. *J. Chem. Phys.* **2005**, *123*, 234905-1−234905-7.
(34) Murat, M.; Grest, G. S.; Kremer, K. *Macromolecules* **1999**, *32*, 595−609.
(35) Tsige, M.; Mattsson, T. R.; Grest, G. S. *Macromolecules* **2004**, *37*, 9132−9138.
(36) Affouard, F.; Kroger, M.; Hess, S. *Phys. Rev. E* **1996**, *54*, 5178−5186.
(37) van Duijneveldt, J. S.; Gil-Villegas, A.; Jackson, G.; Allen, M. P. *J. Chem. Phys.* **2000**, *112*, 9092−9104.
(38) Nicklas, K.; Bopp, P.; Brickmann, J. *J. Chem. Phys.* **1994**, *101*, 3157−3171.
(39) Lin, S.; Numasawa, N.; Nose, T.; Lin, J. *Macromolecules* **2007**, *40*, 1684−1692.
(40) Zimm, B. H. *J. Chem. Phys.* **1948**, *16*, 1099−1116.
(41) Chu, B. *Laser Light Scattering*, 2nd ed.; Academic Press: New York, 1991.
(42) Pecora, R.; Berne, J. *Dynamic Light Scattering*; Plenum Press: New York, 1991.
(43) OCTA Home Page. http://octa.jp.
(44) Bourov, G. K.; Bhattacharya, A. *J. Chem. Phys.* **2003**, *119*, 9219−9225.
(45) Bourov, G. K.; Bhattacharya, A. *J. Chem. Phys.* **2005**, *122*, 044702-1−044702-6.
(46) Grest, G. S.; Kremer, K. *Phys. Rev. A* **1986**, *33*, 3628−3631.
(47) Grest, G. S.; Lacasse, M.-D. *J. Chem. Phys.* **1996**, *105*, 10583−10594.
(48) Cheng, H.; Shen, L.; Wu, C. *Macromolecules* **2006**, *39*, 2325−2329.
(49) Burchard, W.; Schmidt, M.; Stockmayer, W. H. *Macromolecules* **1980**, *13*, 1265−1272.

(50) Douglas, J. F.; Roovers, J.; Freed, K. F. *Macromolecules* **1990**, *23*, 4168−4180.
(51) Vagberg, L. J. M.; Cogan, K. A.; Gast, A. P. *Macromolecules* **1991**, *24*, 1670−1677.
(52) Cho, C.-S.; Nah, J.-W.; Jeong, Y.-I.; Cheon, J.-B.; Asayama, S.; Ise, H.; Akaike, T. *Polymer* **1999**, *40*, 6769−6775.
(53) Klee, W. A. *Biochemistry* **1968**, *7*, 2731−2736.
(54) Quadrifoglio, F.; Urry, D. W. *J. Am. Chem. Soc.* **1968**, *90*, 2755−2760.
(55) Chécot, F.; Lecommandoux, S.; Gnanou, Y.; Klok, H.-A. *Angew. Chem., Int. Ed.* **2002**, *41*, 1340−1343.
(56) Higashi, N.; Koga, T.; Niwa, M. *Adv. Mater.* **2000**, *12*, 1373−1375.
(57) Robinson, C.; Ward, J. C. *Nature* **1957**, *180*, 1183−1184.
(58) Kim, K. T.; Park, C.; Vandermeulen, G. W. M.; Rider, D. A.; Kim, C.; Winnik, M. A.; Manners, I. *Angew. Chem., Int. Ed.* **2005**, *44*, 7964−7968.